PANDA

Three-axis spectrometer

P. Link (TUM), A. Schneidewind

Jülich Centre for Neutron Science
Forschungszentrum Jülich

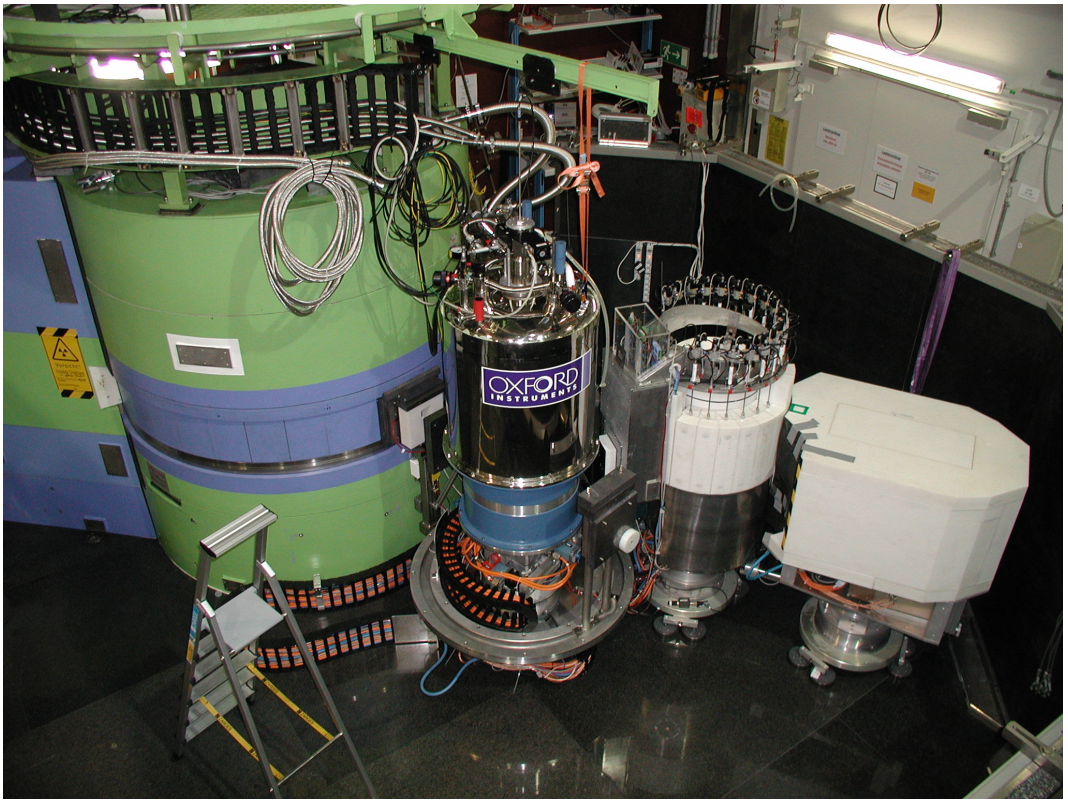

Manual of the JCNS Laboratory Course Neutron Scattering

Contents

1 Introduction and theoretical basics

This summary is thought as a repetition of the basic knowledge needed for this experiment. It is expected to be familiar with the different types of the crystal lattices, the terms of *unit cell* and *basis* as well as the use of *Miller's indices*.

1.1 Inelastic scattering cross section

In the experiment a sample is illuminated by a *monoenergetic* (energy E_i) neutron beam with a *direction* (wave vector $\boldsymbol{k}_i$). The ratio of the intensity scattered in a decent solid angle $d\Omega$ (wave vector $\boldsymbol{k}_f$) with the energy $Ef + dE$ to the intensity of the incoming beam is the differential scattering cross section

$$\frac{I_{\Omega,E_f}}{I_0} = \frac{d\sigma^2}{d\Omega\, dE_f}. \tag{1}$$

The scattering of the neutrons at the nuclei is handled within the quantum mechanics as a weak perturbation of the system. The calculation can be found as "Fermi's golden rule" in the textbooks.Reference: [6]

Generally, the scattering cross section is:

$$\frac{d^3\sigma}{d\Omega\, dE_f} = \frac{|\boldsymbol{k}_f|}{|\boldsymbol{k}_i|} S(\boldsymbol{Q}, \omega). \tag{2}$$

The scattering function S depends on the momentum transfer[1] $\boldsymbol{Q} = \boldsymbol{k}_i - \boldsymbol{k}_f$ and the energy transfer, to be written in a change of the wave length $\omega = \frac{E}{\hbar}$. The relation between ω or E and $|\boldsymbol{k}_f|$ is of squared, therefore the scattering cross section used in 1.9 is for the following calculations (Reference: [11], chap.4):

$$\frac{d^3\sigma}{d\boldsymbol{k}_{fx}\, d\boldsymbol{k}_{fy}\, d\boldsymbol{k}_{fz}} \propto \frac{1}{|\boldsymbol{k}_i|} S(\boldsymbol{Q}, \omega). \tag{3}$$

We start with elastic scattering ($|\boldsymbol{k}_i| = |\boldsymbol{k}_f|$). We will find that this is given by the assumption of a time-independent distribution of the scattering centers.

1.2 Elastic scattering function

We describe the incoming neutron beam as a plane wave. Its amplitude at every time t depends on the site $\boldsymbol{P} = \boldsymbol{R} + \boldsymbol{r}$ (see Fig. 1):

$$\mathcal{A}_P = \mathcal{A}_0\, e^{i[\boldsymbol{k}_i \cdot (\boldsymbol{R}+\boldsymbol{r})] - i\omega_0 t}. \tag{4}$$

It excited the scattering centers to emit spherical waves with an amplitude $\mathcal{A}'$, having a fix phase relation to the original (incident) wave.

$$\mathcal{A}'_P = \rho(\boldsymbol{P})\, \mathcal{A}_P, \tag{5}$$

[1] Really: the change of the wave vector. In units of $\hbar$ this is exactly the momentum transfer.

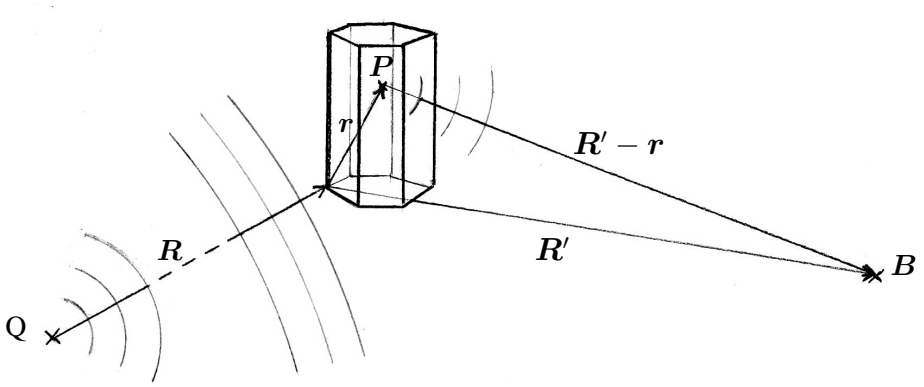

Figure 1: *General scattering geometry and notation*

$\rho(\boldsymbol{r})$ is the local scattering density with the unit m^{-2}. No multiple scattering occurs [2]. At a site $\boldsymbol{B}$ we get for a wave starting from a site $\boldsymbol{P}$:

$$\mathcal{A}_B(\boldsymbol{r},t) = \mathcal{A}_P(\boldsymbol{r},t)\,\rho(\boldsymbol{r})\frac{e^{i[\boldsymbol{k}_f\cdot(\boldsymbol{R'}-\boldsymbol{r})]}}{|\boldsymbol{R'}-\boldsymbol{r}|} \tag{6}$$

where $\boldsymbol{k}_f$ is pointing into the direction of $(\boldsymbol{R'}-\boldsymbol{r})$t.

We assume the distance between R and R' to be large compared to r.

$$\mathcal{A}_B(\boldsymbol{r},t) = \mathcal{A}_P(\boldsymbol{r},t)\,\rho(\boldsymbol{r})\frac{1}{R'}e^{i[\boldsymbol{k}_f\cdot(\boldsymbol{R'}-\boldsymbol{r})]} \tag{7}$$

with the same direction of $\boldsymbol{k}_f$ for all $\boldsymbol{P}$. After replacing $\mathcal{A}_P$ and ordering:

$$\mathcal{A}_B(\boldsymbol{r},t) = \frac{\mathcal{A}_0}{R'}e^{i(\boldsymbol{k}_i\cdot\boldsymbol{R}+\boldsymbol{k}_f\cdot\boldsymbol{R'})}\rho(\boldsymbol{r})e^{-i[(\boldsymbol{k}_f-\boldsymbol{k}_i)\cdot\boldsymbol{r}]-i\omega_i t}. \tag{8}$$

The first term is a constant phase factor, which is now space-independent within the sample. The whole scattering amplitude is given by integration of the scattering region.

$$\mathcal{A}_B(t) \propto e^{-i\omega_i t}\int_V \rho(\boldsymbol{r})e^{-i[(\boldsymbol{k}_f-\boldsymbol{k}_i)\cdot\boldsymbol{r}]}d\boldsymbol{r}. \tag{9}$$

As long as ρ is time-independent, the time dependence of $\mathcal{A}_B$ includes only the frequency ω_i (elastic scattering).

In the experiment, we do not have access to the amplitude of the wave but only to the square of it. For the scattering function one gets:

$$S(\boldsymbol{Q}) \propto \left|\int_V \rho(\boldsymbol{r})e^{-i\,\boldsymbol{Q}\cdot\boldsymbol{r}}d\boldsymbol{r}\right|^2 \tag{10}$$

$$\text{with:}\quad \boldsymbol{Q} = \boldsymbol{k}_f - \boldsymbol{k}_i. \tag{11}$$

Therefore, we identify the scattering function except a factor as the square of the Fourier transform of the scattering density.References: [7], [12]

[2] according to the Born approximation in the quantum-mechanical scattering theory

1.3 Coherent vs. incoherent scattering

Restricting on the interactions with the nuclei and using thermal neutron wavelengths ($\approx$ Å) which are large compared to the radii of the nuclei (10^{-4} Å) the sample can be assumed to be an array of point-shaped scattering centers. The scattering density follows as:

$$\rho(\boldsymbol{r}) = \sum_i b_i \delta(\boldsymbol{r}_i - \boldsymbol{r}) \tag{12}$$

with the positions of the scattering centers $\boldsymbol{r}_i$ and their scattering lengths b_i, respectively. b represents the amplitude of the spherical wave emitted by an atom and $\bar{b}$ its average.

The scattering function of a material with identical atoms in regular order is again a regular point lattice (see next chapter). But, a normal crystal is a mixture of several isotopes having different neutron scattering lengths. In this case, the interference condition is valid only for an averaged scattering length. Taking (12) for (10), the scattering function is s

$$S = \left(\bar{b}\right)^2 S_{\text{coh.}} + \left(\bar{b}^2 - \left(\bar{b}\right)^2\right) S_{\text{inc.}}. \tag{13}$$

assuming a statistical distribution of the different scattering centers. $S_{\text{inc.}}$ is now independent of the relative positions of the atoms to each other and therefore independent of the concrete structure of the sample. It is a term of background signal, independent of the scattering angle and the sample orientation. This so-called incoherent scattering is always observed when the scattering density varies locally and non-correlated, also for point defects in the lattice and randomly distributed spin orientations in nuclei and atomic shells. A distinguished incoherent scatterer - almost without a coherent distribution - is vanadium which is often used for spectrometer alignments. Reference: [12]

1.4 Reciprocal space and Brillouin-zones

The samples to be investigated are normally good coherent scatterers, it is necessary to know $S_{\text{coh.}}$. Let's start on a Bravais-lattice with a one-atom basis. The scattering density is:

$$\rho(\boldsymbol{r}) = \sum_{h,k,l} b\ \delta^3[(h\,\boldsymbol{a}_1 + k\,\boldsymbol{a}_2 + l\,\boldsymbol{a}_3) - \boldsymbol{r}], \tag{14}$$

with generating lattice vectors $\boldsymbol{a}_i$. The Fourier transform of such a function is:

$$\tilde{\rho}(\boldsymbol{q}) = \frac{1}{\sqrt{2\pi}} \int \sum_{h,k,l} b\ \delta^3[(h\,\boldsymbol{a}_1 + k\,\boldsymbol{a}_2 + l\,\boldsymbol{a}_3) - \boldsymbol{r}] e^{-i\boldsymbol{q}\cdot\boldsymbol{r}} d\boldsymbol{r} \tag{15}$$

$$= \sum_{h,k,l} b e^{-i\boldsymbol{q}\cdot[(h\,\boldsymbol{a}_1 + k\,\boldsymbol{a}_2 + l\,\boldsymbol{a}_3)]}. \tag{16}$$

Summarizing for a sufficient number of indices, one gets a point lattice again, the *reciprocal lattice* [3]. The wave vector space is named the *reciprocal space*.

[3] It can be shown that the reciprocal lattice of a Bravais lattice is a Bravais lattice again having all symmetry elements of the original lattice.

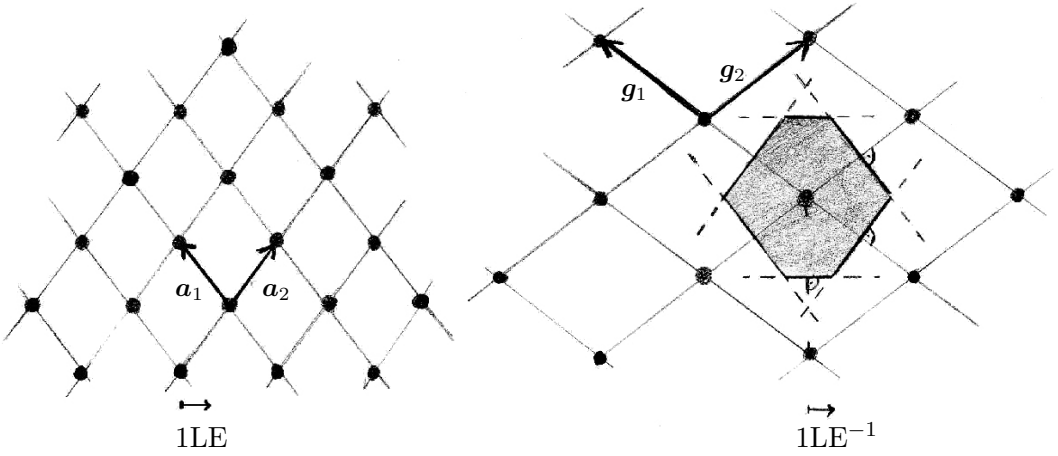

Figure 2: *2-dimensional point lattice in the real and reciprocal spaces. The first Brillouin zone is plotted around a reciprocal lattice point. Note the generating vectors of both lattices satisfying equation (17).*

By

$$\boldsymbol{g}_i \cdot \boldsymbol{a}_j = 2\pi\delta_{i,j} \tag{17}$$

we get the generating vectors $\boldsymbol{g_i}$ of the reciprocal space from the original vectors [4]: The reciprocal lattice vector $\boldsymbol{g_1}$ is perpendicular to the vectors $\boldsymbol{a_2}$ and $\boldsymbol{a_3}$ with an absolute value of:

$$\frac{2\pi}{(a_1 \cos \sphericalangle(\boldsymbol{a}_1, (\boldsymbol{a}_2 \times \boldsymbol{a}_3)))}. \tag{18}$$

In the simple case of the sc lattice all real lattice vectors are pairwise perpendicular. Thus, the directions of the reciprocal space are identical to that of the real space. But, the dimensions of the reciprocal lattice as well as of the wave vectors are'm^{-1}' (see eq. (17)).

In (10) we identified the scattering function as the square of the Fourier transformed of the scattering density. It is different from zero if

$$\boldsymbol{Q} = \boldsymbol{G} = h\boldsymbol{g}_1 + k\boldsymbol{g}_2 + l\boldsymbol{g}_3 \qquad \text{(Laue condition)}. \tag{19}$$

Wave vectors satisfying this condition built the Bragg reflections in the sample spectrum and are enumerated by the indices h, k, l.

fcc and bcc lattices are normally not presented by their primitive unit cells but as sc lattices with a polyatomic basis. Therefore, not all reflections of the sc lattice occur. This is described by the *structure factor*. Here eq. (17) does not give the generating wave vectors of the reciprocal space.

A useful construction to work with the wave vectors of the reciprocal space is the construction of the Brillouin zones. For this, in the reciprocal lattice the perpendicular bisector planes of the vectors connecting one lattice point with all the others are created. [5] (see also Fig. 2).

[4] The definition (17) is used in physics. The 2π factor depends on the definition of the wave vector and is sometimes omitted, especially in crystallography.

[5] All incoming plane waves with wave vectors ending at the Brillouin zone boundary satisfy the elastic scattering condition (19) since incident and final wave vector are of the same length.

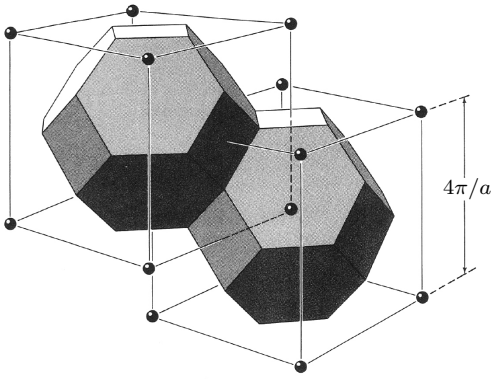

(a) The reciprocal lattice of a fcc crystals is a bcc lattice. The first two Brillouin zones are drawn. If the crystal consists of two interlocking fcc lattices (i.e. Silicon), not all reflections occur.

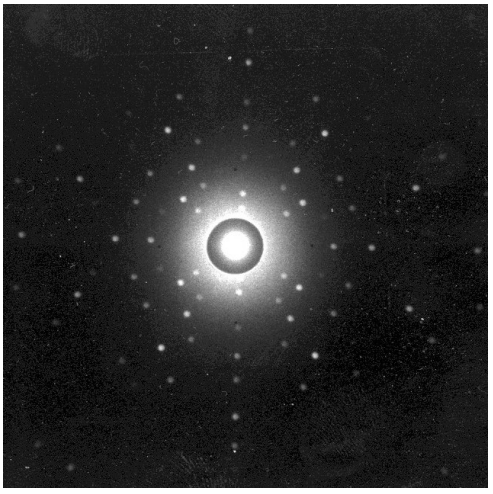

(b) Laue picture of a Silicon crystal ([110]-direction) irradiated by polychromatic x-rays. We get a two-dimensional projection of the reciprocal lattice up to decent indices, depending on the minimum wavelength of the x-rays.

Figure 3: *3-dimensional view of the elastic scattering.*

Remark: The construction of the Brillouin zones is of the basis Bravais lattice. I.e., Germanium and Silicon have a fcc lattice with a 2-atomic basis. The scattering function in influenced in a way that several refections vanish, others are amplified. The reciprocal lattice stays to be of fcc symmetry.

The first Brillouin zones around the points of the reciprocal lattice fill the reciprocal space. By this, points of high symmetry are easy to identify. They are used to be named by letters (see Fig. 6).

References: [7] Chapter about scattering on periodic structures.

1.5 Inelastic scattering processes

We allow a change of the scattering density ρ with time now.

$$\rho(\boldsymbol{r}(t)) \propto \sum_n \delta(\boldsymbol{r}_n(t) - \boldsymbol{r}). \tag{20}$$

The atoms are oscillating with weak amplitudes around their average position.

$$\boldsymbol{r}_n(t) = \boldsymbol{r}_n + \boldsymbol{u}_n(t). \tag{21}$$

Assuming the forces between neighboring atoms to be proportional to their displacement (harmonic approximation) every oscillation state of the crystal can be described as a superposition

of plane waves with wave vectors $\boldsymbol{q}$. [6]:

$$\boldsymbol{u}_n(t) = \sum_{\boldsymbol{q}} \boldsymbol{u}\, e^{\pm i(\boldsymbol{q}\cdot\boldsymbol{r}_n - \omega(\boldsymbol{q})\, t)}. \tag{22}$$

The scattering amplitude is from (10) and (20):

$$\mathcal{A} \propto e^{-i\omega_i t} \sum_n e^{-i\,\boldsymbol{Q}\cdot\boldsymbol{r}_n(t)}. \tag{23}$$

Take eq. (21) to develop the exponential function for small u's:

$$\mathcal{A} \propto e^{-i\omega_i t} \sum_n e^{-i\,\boldsymbol{Q}\cdot\boldsymbol{r}_n} e^{-i\,\boldsymbol{Q}\cdot\boldsymbol{u}_n(t)} \tag{24}$$

$$\approx e^{-i\omega_i t} \sum_n e^{-i\,\boldsymbol{Q}\cdot\boldsymbol{r}_n} [1 - i\,\boldsymbol{Q}\cdot\boldsymbol{u}(t)] \tag{25}$$

$$= e^{-i\omega_i t} \sum_{n,\boldsymbol{q}} e^{-i\,\boldsymbol{Q}\cdot\boldsymbol{r}_n} - i\,\boldsymbol{Q}\cdot\boldsymbol{u}\, e^{-i\,\boldsymbol{Q}\cdot\boldsymbol{r}_n} e^{\pm i(\boldsymbol{q}\cdot\boldsymbol{r}_n - \omega(\boldsymbol{q})\, t)}. \tag{26}$$

In (26) we find in addition to the terms from elastic scattering for every $\boldsymbol{q}$ a term:

$$\sum_n i\,\boldsymbol{Q}\cdot\boldsymbol{u}\, e^{-i[(\boldsymbol{Q}\mp\boldsymbol{q})\cdot\boldsymbol{r}_n] - i[\omega_i \pm \omega(\boldsymbol{q})]t}. \tag{27}$$

Thus, there are scattering waves with frequencies shifted from the frequency of the primary wave just by the frequency of the crystal oscillations. In addition, in analogy to the elastic case, the sum in (27) is non-zero only if eq.

$$\boldsymbol{Q} = \boldsymbol{k}_i - \boldsymbol{k}_f = \boldsymbol{G} \mp \boldsymbol{q} \tag{28}$$

is satisfied by a reciprocal wave vector $\boldsymbol{G}$. The condition for the frequency is:

$$\omega_f = \omega_i \pm \omega(\boldsymbol{q}). \tag{29}$$

Multiplying both equations with $\hbar$ and choosing $\boldsymbol{G} = 0$ gives:

$$\hbar\Delta\omega \mp \hbar\omega(\boldsymbol{q}) = 0, \tag{30}$$

$$\hbar\boldsymbol{k}_f - \hbar\boldsymbol{k}_i \mp \hbar\boldsymbol{q} = 0. \tag{31}$$

This is just the quantum-mechanical description of the momentum and energy conservation for neutron scattering on a particle generally called a *phonon*. The analogy is confirmed also quantum-mechanically.

See i.e. [1] appendix N.

As to be seen from the equation, the momentum of a phonon is determined only modulo to one reciprocal lattice vector. Really two lattice oscillations of wave vectors differing by one

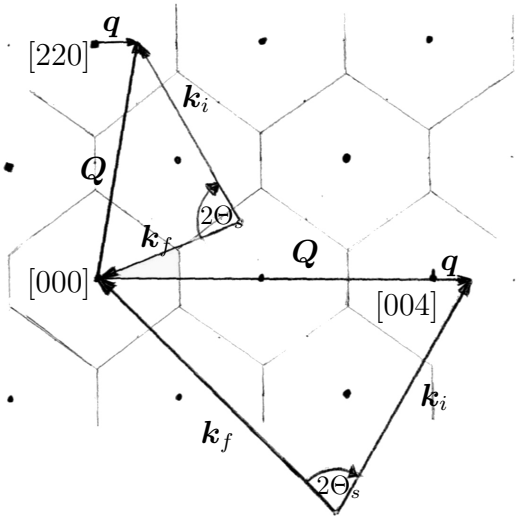

Figure 4: *Scattering diagrams for inelastic scattering of neutrons on a fcc crystal. The reciprocal* $[1\bar{1}0]$ *plane is drawn. Notation similar to the text. The energy transfer is represented by the different lengths of* $\mathsf{k_i}$ *and* $\mathsf{k_f}$

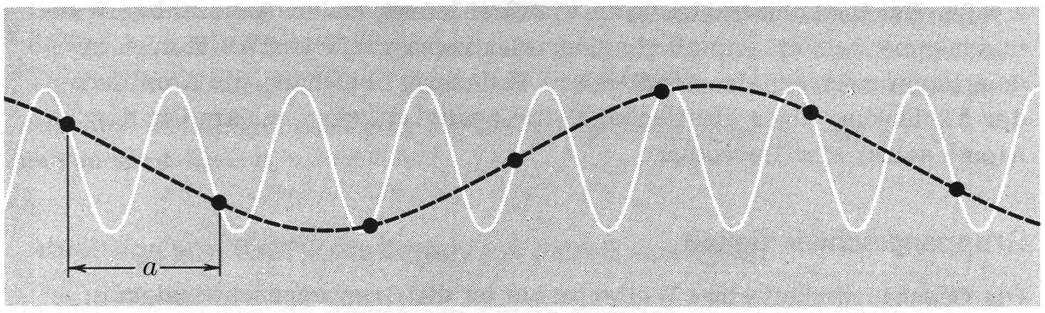

Figure 5: *Equivalence of lattice vibrations taken from [9]: Both of the shown waveslead to the same displacement of the atoms from their avarage position. They are physically identical. All waves with a wavelength* λ_1 *smaller than* $2\mathsf{a}$ *(white line) can be reduced to these with* $\lambda_2 \geq 2\mathsf{a}$ *(black line).* $\frac{2\pi}{\lambda_1} = \frac{2\pi}{\lambda_2} - \mathsf{n}\frac{2\pi}{\mathsf{a}}$*, with* $\mathsf{n}\frac{2\pi}{\mathsf{a}}$ *the length of a reciprocal lattice vector. The waves with* $\lambda \geq 2\mathsf{a}$ *are just these with wavevectors in the first Brilloin zone.*

reciprocal lattice vectors are similar by physics (see fig. 5). Thus, the wave vector of every phonon can be related to the nearest reciprocal lattice point and the theoretical considerations are restricted to the 1. Brillouin zone. The probability of the excitation of a phonon scales with the intensity of the nearest elastic reflection. See for example fig. 9. Phonons are therefore particles with a quasi-momentum [7].

Reference: see [7] chapter 4

For the visualization of the inelastic scattering process one can assume that the neutron initiates an oscillation in the crystal. By this, the neutron looses energy or gains energy when scattered on an oscillating atom which results in the annihilation of this oscillation. For the energy loss, a decent mode has to be already excited in the crystal. Such a consideration of the energies leads to the "'detailed balance"' principle:

$$S(\boldsymbol{Q}, -\omega) = e^{-\frac{\hbar\omega}{k_B T}}\ S(\boldsymbol{Q}, \omega) \tag{32}$$

with the Boltzmann factor $k_B T$. At room temperature, both sides are almost equivalent.

What is now the advantage of neutrons for the study of lattice vibrations, compared to x-rays - which are easier to handle and available with much higher flux, especially at synchrotron sources where in addition higher brilliance is achieved? The energy of thermal neutrons is in average circa $30\,\mathrm{meV}$ which is related to a wavevector of $3.8\,\mathrm{\AA}^{-1}$. The dimensions of the reciprocal space are given by eq. (17), i.e. circa $2\,\mathrm{\AA}^{-1}$ for Germanium. X-rays with similar wave vectors have energies of $\approx 10\,\mathrm{keV}$. The excitation of a lattice vibration with an energy of $10\,\mathrm{meV}$ would be according to a relative energy change of 10^{-6} for photons. For neutrons the change is in the order of kinetic energies.

1.6 Dispersion relation

One purpose of the experiment is to determine the correlation $\omega(\boldsymbol{q})$ experimentally. $\omega(\boldsymbol{q})$ is the (phonon) dispersion relation. It contains all information about the dynamic properties of the studied material. Physical quantities as velocity of sound and the phonon contribution of the heat capacity can be deduced from it. But, also the dominating interaction potentials between the atoms can be derived. For the visualization the 3-dimensional relation is drawn for several directions of symmetry abreast.

The principle of $\omega(\boldsymbol{q})$ can be shown at an one-dimensional atomic chain. See the textbook derivation (i.e. [1]). The generalization is done by the transition to parallel crystal planes oscillating contrary.

---

[6] This is the first-order Taylor series approximation of anharmonic potentials.

[7] The real momentum transfer of the neutrons is - as for elastic scattering - absorbed by the whole sample and is not relevant due to the mass ratio.

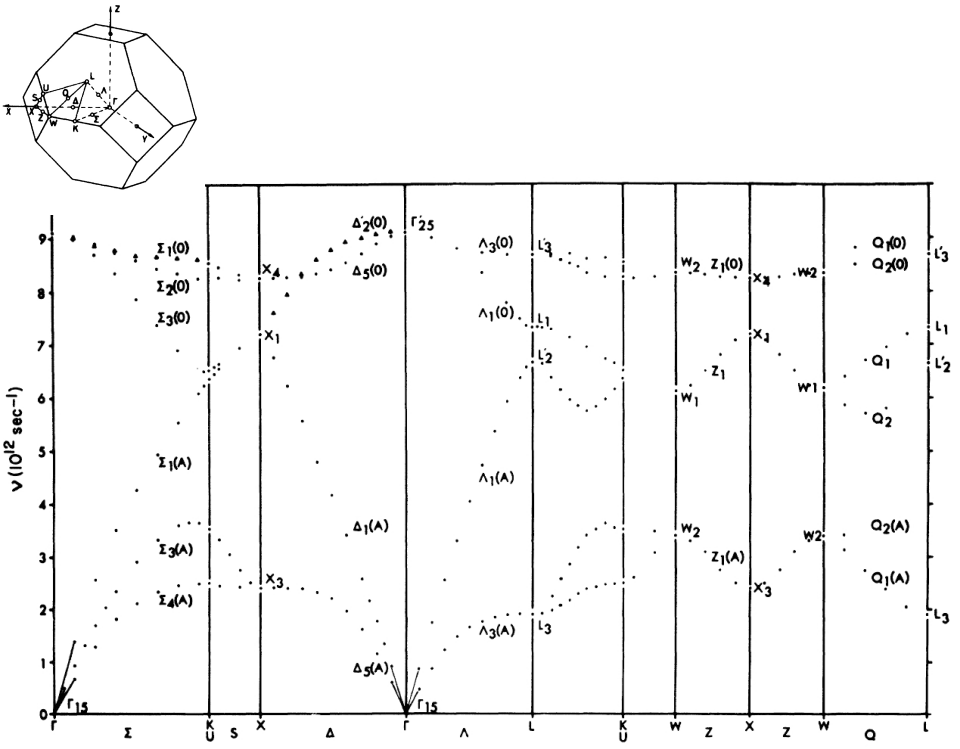

Figure 6: *Dispersion relation of Germanium at 80 K taken from [10]. Points of exceptionally high symmetry are indicated by letters. (small picture).*

1.7 Transverse and longitudinal phonons

As known from mechanics, for propagating waves the displacement of the single atoms can be chosen parallel (longitudinal) or perpendicular (transversal) to the propagation direction. In general, both excitation have different energies. For every $\boldsymbol{q}$ there are two transverse phonons with polarizations perpendicular to each other, but only one of them is in the scattering plane. In crystals of high symmetry these excitations are degenerated in energy. A crystal with a one-atomic basis has three dispersion modes. For a basis of n atoms,this number increases to $3n$ (3 acoustic ($E = 0$ in the center of the B-zone) and $3(n-1)$ optical modes ($E \neq 0$ at $q = 0$)). Fig. 6 shows this for the simple case of Germanium.

Reference: [9]

How can transverse and longitudinal oscillations to be distinguished in the experiment? The equation of the inelastic scattering function (27) contains the scalar product $\boldsymbol{Q} \cdot \boldsymbol{u}$ with the polarization of the wave $\boldsymbol{u}$ (fig. 7). Thus, an oscillation is only excited for $\boldsymbol{Q}$ with a component in the polarization direction, in analogy to the classical assumption. Fig. 4 shows the measurement of a longitudinal and of a transverse phonon. The wave vector $\boldsymbol{q}$ points in the same direction for both measurements.

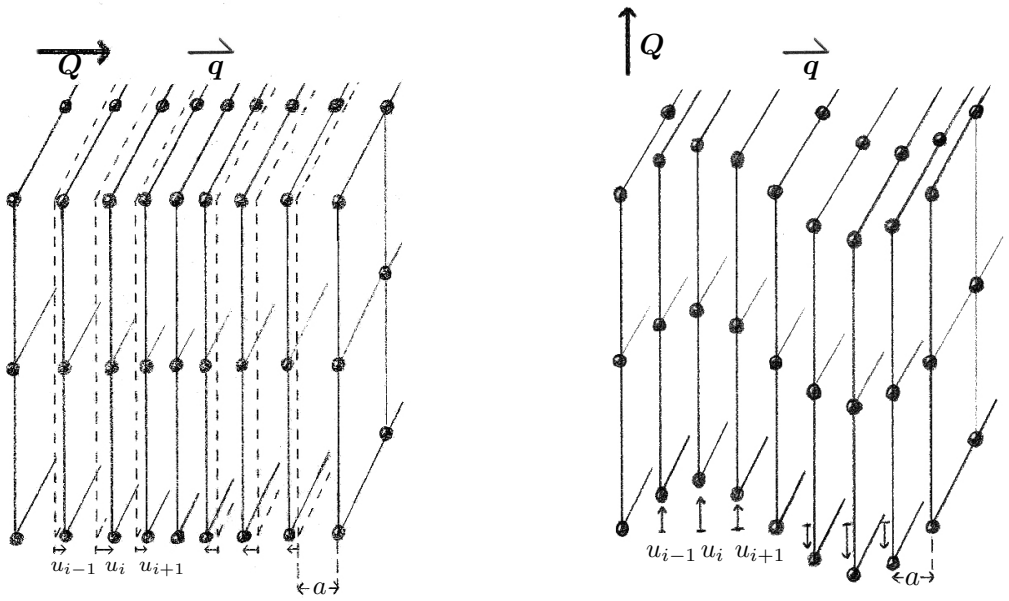

(a) longitudinal... (b) and transversal oscillations

Figure 7: *Note: The momentum transfer of the neutrons* Q *points always into the direction of the real displacements* u_i.

1.8 What is measured - what can we conclude for the sample

We look now at the correlation between the configuration of the spectrometer and the variables $\boldsymbol{Q}$ and ΔE. The absolute values of $\boldsymbol{k}_i$ and $\boldsymbol{k}_f$ (incident and outgoing wave vectors) are determined by the scattering angles at the monochromator and the analyzer crystals $2\Theta_m$ and $2\Theta_a$, respectively [8]. Having neutron waves we need

$$E_{\text{kin}} = \frac{(\hbar\, k_{\text{n}})^2}{2m}\ , \tag{33}$$

with $\boldsymbol{p}$ the momentum and m the mass of the neutron.
Thus, we know also

$$\omega = \frac{\Delta E}{\hbar} = \hbar\,\frac{|\boldsymbol{k}_i|^2 - |\boldsymbol{k}_f|^2}{2\,m_{\text{n}}}. \tag{34}$$

The orientation of the sample determines the direction of $\boldsymbol{k}_i$ relatively to the crystal lattice (characterized by the sample rotation angle ω_s) and the scattering plane. Within the scattering plane $2\Theta_s$ determines the direction of $\boldsymbol{k}_f$. $\boldsymbol{Q}$ results from eq. (11).

Conversely, we do not get the configuration of the instrument from ω and $\boldsymbol{Q}$.

In standard experiments, the scans are done at constant $\boldsymbol{Q}$ or constant energy transfer ΔE. While for very stiff dispersion modes, in the vicinity of the Brillouin zone center, constant-E is chosen (Fig. 8(b)), most of the Brillouin zone is normally measured with const.-$\boldsymbol{Q}$ (Fig. 8(a)).

[8] $2\Theta_m$ and $2\Theta_a$ are the relevant numbers. The rotation of the crystals Θ_m and Θ_a are fixed in relation to $2\Theta_m/2$ and $2\Theta_a/2$.

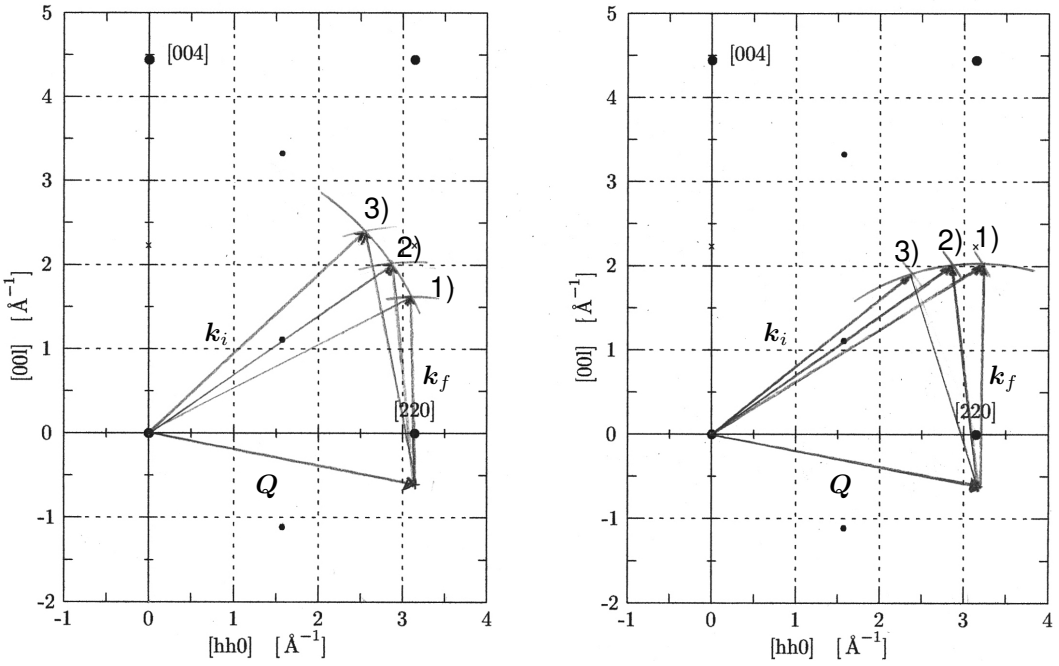

(a) Example for constant-Q scans

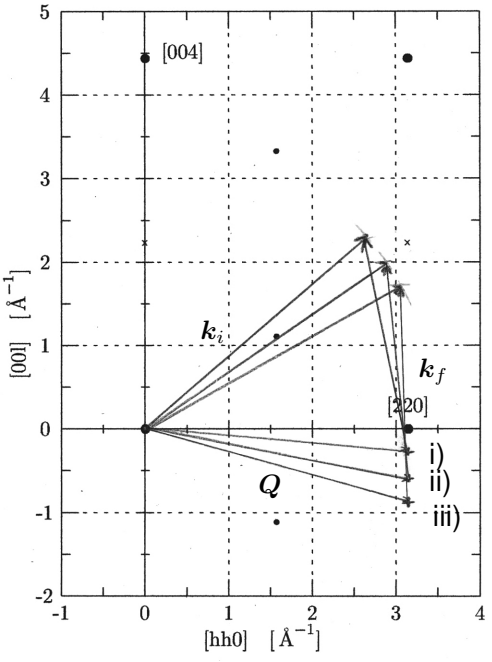

(b) A constant-E scan

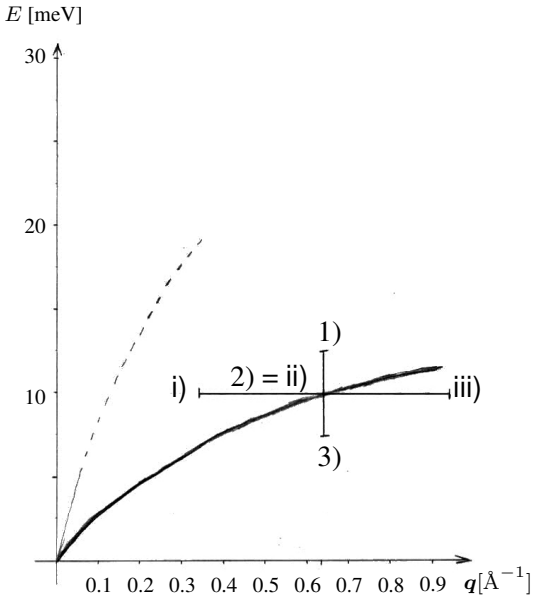

(c) corresponding points of the dispersion relation

Figure 8: *Examples for different scans (scattering triangles and dispersion relation.)*

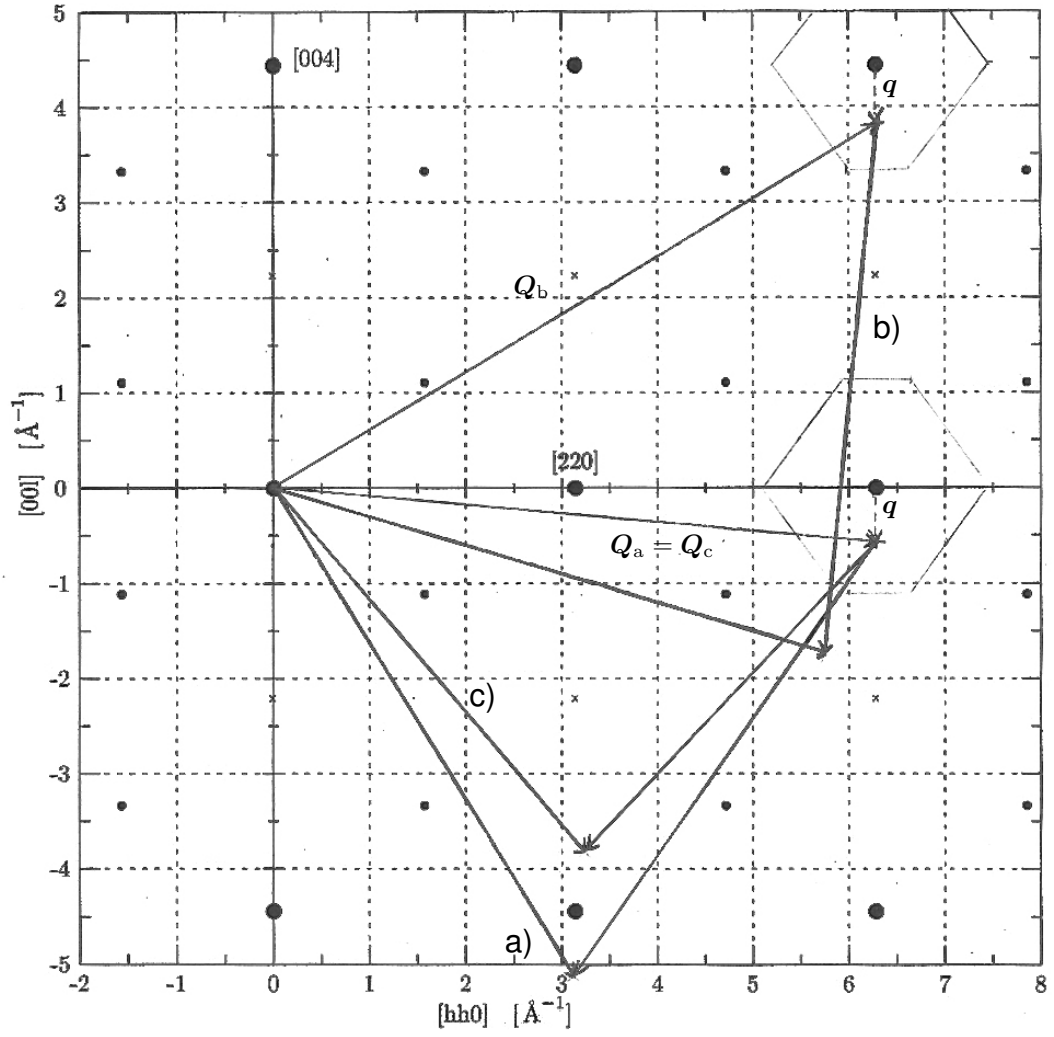

Figure 9: *The same phonon excitation measured in different ways:*
(a)↔(b): Measurements at different elastic peaks but with identical $|\boldsymbol{k}_i|$ *and* $|\boldsymbol{k}_f|$.
(a)↔(c): Identical position of the reciprocal space measured with different $\boldsymbol{k}_i$.

Please take time and think about the reason and how the different angles change during the two measurements shown in the figures.

As demonstrated in fig. 9, the lengths of $\boldsymbol{k}_i$ or $\boldsymbol{k}_f$ can be fixed. This is a way to change the resolution of the instrument optimizing the measurement for different problems.

1.9 Normalization of the counting rates

Planning an experiment, it seems to be native to count the scattered neutrons in the detector at every point for a useful time. But, the counting rate Z_{Det} depends not only on the scattering cross section. It also depends on instrument parameters which possibly change during the measurement or within a scan.

$$Z_{\mathrm{Det}} \propto I_{\mathrm{prim}}(\boldsymbol{k}_i) \cdot R_{\mathrm{Mono}}(|\boldsymbol{k}_i|) \; \frac{d^3\sigma}{d\boldsymbol{k}_{fx}\, d\boldsymbol{k}_{fy}\, d\boldsymbol{k}_{fz}} \; R_{\mathrm{Anal}}(|\boldsymbol{k}_f|) \cdot P_{\mathrm{Det.}}(|\boldsymbol{k}_f|) \tag{35}$$

$$= I_{\mathrm{prim}}(\boldsymbol{k}_i) \cdot R_{\mathrm{Mono}}(|\boldsymbol{k}_i|) \; \frac{1}{|\boldsymbol{k}_i|} \; S(\boldsymbol{Q},\omega) \; R_{\mathrm{Anal}}(|\boldsymbol{k}_f|) \cdot P_{\mathrm{Det.}}(|\boldsymbol{k}_f|). \tag{36}$$

with $R(|\boldsymbol{k}|)$ the reflectivities of the Bragg crystals, $P_{\mathrm{Det.}}(|\boldsymbol{k}_f|)$ the efficiency of the detector and $I_{\mathrm{prim.}}(|\boldsymbol{k}_i|)$ the incident intensity at the used energy.

In our experiment here we are especially interested at the *positions* of the phonon excitations in the $\boldsymbol{Q}$-ωspace and not too much in their intensities. We therefore do not ask for the comparability of *different* scans. We only need sufficient count rates *within* the scans and possibly the normalization of different points in a scan to determine the peak position in a right way.

We use a monitor detector usually mounted after the monochromator and before the sample. The probability to be detected is for neutrons with a velocity v proportional to the time t the neutrons stay in a detector (monitor) of the width d:

$$t = \frac{d}{v} = \frac{d\, m_{\mathrm{n}}}{\hbar\, |\boldsymbol{k}|} \tag{37}$$

One expects as monitor count-rate:

$$Z_{\mathrm{Mono}} \propto I_{\mathrm{prim}}(\boldsymbol{k}_i) \cdot R_{\mathrm{Mono}}(|\boldsymbol{k}_i|) \frac{1}{|\boldsymbol{k}_i|} \tag{38}$$

To perform a measurement, events are counted in the detector until a particular number of monitor counts is reached. The real count rate in the detector with monitor Z'_{Det} is:

$$Z'_{\mathrm{Det}} = \frac{Z_{\mathrm{Det}}}{Z_{\mathrm{Moni}}} \propto S(\boldsymbol{Q},\omega) \; R_{\mathrm{Anal}}(|\boldsymbol{k}_f|) \cdot P_{\mathrm{Det.}}(\boldsymbol{k}_f). \tag{39}$$

For constant $|\boldsymbol{k}_f|$, as illustrated in fig. 8(a)(right), this dependence vanishes. This is therefore the common mode. If $|\boldsymbol{k}_f|$ is varied by any reasons during the scan, the corresponding corrections have to be done for the data analysis.

1.10 Resolution function

Up to now we did not consider the fact that at every point of the $\boldsymbol{Q}$-ω-space the spectrometer is pointing to the measured intensity is scattered in a finite volume around this point. A sharp (δ-) peak in the scattering function at $(\boldsymbol{Q}_0, \omega_0)$ gives a measured signal of the form:

$$Z_{\mathrm{Det}}(\boldsymbol{Q}, \omega) \propto R(\boldsymbol{Q} - \boldsymbol{Q}_0, \omega - \omega_0). \tag{40}$$

R is the *resolution function* and depends on the configuration of the spectrometer only. Ordinary R is assumed to be Gaussian in its components.

The measured signal results from the convolution:

$$Z_{\mathrm{Det}}(\boldsymbol{Q}, \omega) \propto \int S(\boldsymbol{Q}', \omega')\, R(\boldsymbol{Q}' - \boldsymbol{Q}, \omega' - \omega)\, d\boldsymbol{Q}' d\omega'. \tag{41}$$

For illustration take a contour line of the resolution function (exactly: the 2-dimensional projection of the resolution function). It is normally elliptically and shows the region of the scattering function 'seen' by the instrument. In fig. 10 the projections of the resolution function are plotted into the dispersion relation, at the right the intensities to be expected, respectively. A measurement is characterized to be *focused* if the short axes of the resolution ellipsoid is perpendicular to the dispersion surface (to be measured).

It is important to understand in which cases a sharp resolution function is helpful or not. E. g., see a const.-Q-scan through a sharp 'horizontal' dispersion surface:

$$S(\boldsymbol{Q}, \omega) = S_0\, \delta(\omega - \omega_0). \tag{42}$$

The measurement is focused, i.e.

$$R(\boldsymbol{Q}, \omega) = e^{-\frac{\omega^2}{\sigma_\omega}} \cdot R(\boldsymbol{Q}). \tag{43}$$

Eq.(41) gives:

$$Z(\omega) \propto e^{-\frac{\omega^2}{\sigma_\omega}} \int R(\boldsymbol{Q}) d\boldsymbol{Q}. \tag{44}$$

Expanding the resolution ellipsoid in the momentum coordinates, the measured intensity increases. The line width depends only on $e^{-\frac{\omega^2}{\sigma_\omega}}$.

Reference: [11] Chap.4

The real form of the resolution function is influenced now by several effects: The Bragg-crystals are not of perfect lattices but have a finite mosaicity (which means it consists of several small single crystals, and their lattice parameters have weak deviations from the average). This 'mosaicity spread' - given by the angle η_m - broadens the Bragg peaks e.g. at the monochromator. Further influences are the finite angle resolution of the detectors, a finite size of the sample and diverging beams.

The beam reflected at the monochromator is a bunch of wave-vectors with a distribution $p_m(\boldsymbol{k}_i)$, the transmission function of the monochromator. The analyzer has to be described in analogy.

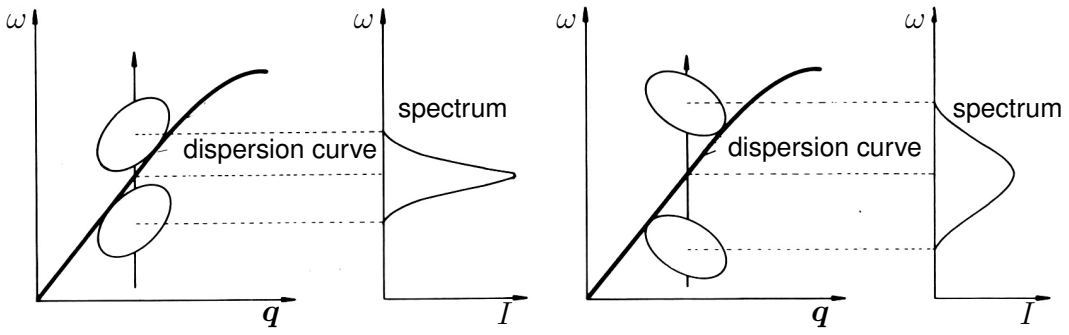

Figure 10: *Focused vs. unfocused measurement.*

To calculate the resolution function of the spectrometer, the two transmission functions have to be convoluted with respect to $2\Theta_s$. This simulation can be done by software tools. You will get some qualitative ideas about this within the experiment.

Reference: [4]

1.11 Peak forms

We learned: For sharp peaks in the scattering function we get a Gaussian signal in the measurement. This will be found in most of the experiments. However, some compounds exhibit broadened phonon resonances, so-called *soft modes*. They are originated by phonon-phonon- and phonon-electron-interactions [9] and result in a finite lifetime τ of the single oscillation states. Calculating the damped harmonic oscillator the line shape is identified to be Lorentzian:

$$S(\omega) \propto \frac{\omega^2}{\left(\omega_0^2 - \omega^2\right)^2 + \left(\frac{\omega}{\tau}\right)^2} \tag{45}$$

with the line width (FWHM):

$$\delta\omega = \frac{1}{2\tau}. \tag{46}$$

The resulting signal of such a 'soft' peak is the convolution of a Lorentzian with a Gaussian curve called Voigt profile. This profile is not easy to be calculated mathematically. In the case of comparable widths of the single profiles it can be sufficient to take the width of the Voigt curve as the sum of the widths of the Gaussian and the Lorentzian contributions.

If it is necessary for the data analysis to determine the peak *widths*, the resolution function has to be deconvoluted from the measured signal. This can be done by software.

Reference: [3], [5]

[9] These effects are neglected by the assumption of harmonic oscillations.

2 Performance of the experiment

PANDA is a three axis spectrometer (TAS) at the cold source of FRM II. The first thermal TAS was built 1954 and generally improved 1959 by Bertram N. Brockhouse at NRU Reactor in Chalk River. For his merit in the field of inelastic neutron scattering he got the Nobel price 1994. Even if the intensities at the detector were increased by magnitudes, the instrument is remote controlled and the safety is improved today, the general principle of the method is still the same:

The beam of cold neutrons (energy $E \approx 5(30)\,\mathrm{meV}$, momentum $p \approx 1.5(4) \cdot 10^{-24}\,\mathrm{kg\,m/s}$), which has de Broglie wavelength

$$\lambda = \frac{h}{p}, \tag{47}$$

or a wavevector of the length $k = \frac{2\pi}{\lambda}$, exits the moderator tank of the reactor through a beam port. The neutrons enter a monochromator being of single crystals with a d-spacing d.

By the Bragg equation

$$n\lambda = 2d \sin \Theta_m \tag{48}$$

the angle $2\Theta_m$ defines the energy of a monochromatic neutron beam (wave vector $\boldsymbol{k}_i$, energy E_i), which points to the sample to be investigated.

Direction and energy of the neutrons are changed at the sample following the inelastic scattering laws. At the secondary spectrometer (analyzer) neutrons with the wave vector $\boldsymbol{k}_f$ and the energy E_f are selected by Bragg reflection at a second crystal and are counted in the detector. By this, the momentum transfer ($\boldsymbol{Q}$) of the neutrons to the sample as well as the energy transfer (ΔE) from the sample to the neutrons can be determined.

$$\boldsymbol{Q} = \boldsymbol{k}_i - \boldsymbol{k}_f, \qquad \Delta E = E_i - E_f. \tag{49}$$

For useful statistics normally a fixed configuration of the instrument - related to a decent energy and momentum transfer - is taken for counting at the detector. The scattering function of the sample is therefore taken pointwise. These scans are measured at constant $\boldsymbol{Q}$ or at constant energy E, depending on the experimental strategy (see below).

PANDA is located at the beamport SR2 in the experimental hall of FRM II and has a comparably large neutron flux at low background. For more detail see:
`http://www.mlz-garching.de/panda`.

We now discuss the components of the three axis spectrometer. Photos of the main components are collected at the gallery 22 for better understanding.

Shielding Since neutrons damage biological matter the region of the primary beam has to be shielded. This is done by a so-called drum (in the case of PANDA blue / green colored) with the monochromator in its centre. The drum is made of heavy concrete with a large amount of chemically combined water, boron added. Also used are boron-treated (PE) sheets. Chemically combined water and PE contain a large amount of hydrogen which is able to decelerate fast

Notation:

$\mathcal{Q}$	Neutron source
$\mathcal{M}$	Monochromator
$\mathcal{S}$	Sample table
$\mathcal{A}$	Analyzer
$\mathcal{D}$	Detector
$\alpha 1$ $\alpha 2$ $\alpha 3$ $\alpha 4$	collimators
$2\Theta_m$ $2\Theta_s$ $2\Theta_a$	angles of the Spectrometer-axis
Abs	Shielding
Sel	Selector
Mob	Mobile blocks
Sh	Primary shutter

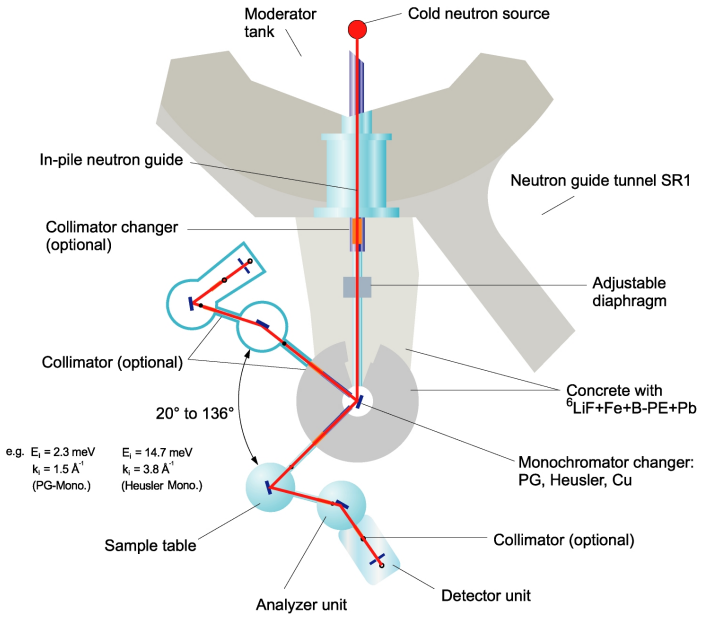

Figure 11: *Schematic design of a three axis spectrometer.*
Remark: all angles are counted in the region $[-180°, 180°]$. (0° is directed in beam, positive angles are counter-clockwise.) $2\Theta_s$ is therefore positive.

neutrons. Boron as a large absorption coefficient for cold and thermal neutrons [10], and the isotope emerging at the neutron capture is not radioactive. But, normally materials are activated by the nuclear reactions and therefore activated (and the reactor emits hard Gamma radiation also if the primary shutter is closed), so the shielding has to be opened only after measurements of the remaining radiation even if the reactor is down. A part of the installation is shown here at the photos. The drum is made to shield γ-radiation as well as neutrons.

During the movement of the monochromator axes a ring of the shielding which contains the beam channel for the beam scatered at the monochromator is entrained. To avoid a closing of the primary beam during the ongoing rotation, the ring partially consists of 11 so-called mobile blocks (made of the same concrete as the ring) which are moved by an automatic control from one side of the opening to the the other. The geometry and the control ensure a proper shielding where necessary (see fig.11).

Monochromator In the rotation centre of the shielding the monochromator is positioned. It consists of 121 single crystals of pyrolytic graphite (PG) mounted on a crystal holder. The crystal holder and therfore the grapite lattice planes are rotated by the angle Θ_m to the primary beam. The intensity of the monochromatic beam scattered at the angle $2\Theta_m$ [11] depends on the lattice parameter of the monochromator material (here PG) and on the incoming angle..

To avoid contamination of higher-order Bragg reflection in the incoming beam, $n = 2, 3 \ldots$ (Gl. (48)), filter materials are positioned between monochromator and sample. In the case of

[10] Typical reaction: $^{10}_{5}\mathrm{B} + ^{1}_{0}\mathrm{n} \rightarrow ^{7}_{3}\mathrm{Li} + ^{4}_{2}\mathrm{He} + 2.8\,\mathrm{Mev}$

[11] Remark: Sometimes the angles Θ_m, Θ_s and Θ_a are named α_1 to α_3.

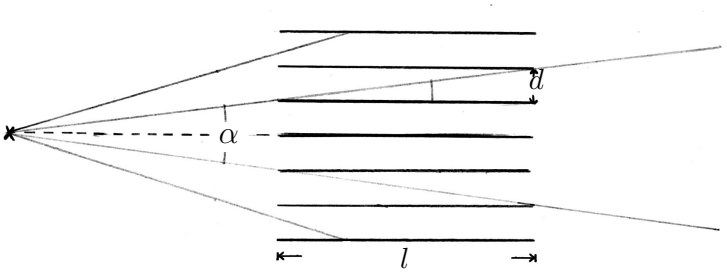

Figure 12: *Drawing of a Soller collimator. The divergence of the outgoing beam is* $\tan(\alpha/2) = \mathsf{d}/\mathsf{l}$*, which is in the example ca.* 18°*. On PANDA the collimation can be chosen between 15 and 80 minutes.*

PANDA this is polycrystalline boron or, sometimes, pyrolytic graphite.

Maximum intensity at sample and detector can be achieved by focusing the monochromator and the analyzer in horizontal and vertical direction. Here the 121 monochromator (55 analyzer) crystals are curved in both directions by complex mechanics to get the crystal surfaces into a paraboloid-like shape. The radius of the curvature depends on the neutron wavelength. By taking into account the distances also a focus of the momentums is possible.

Sample table The sample is mounted on a table which can be moved on air-pressure. In addition to motors rotating the sample and the analyzer/detector around the sample - giving Θ_s and the scattering angle $2\Theta_s$, the sample orientation can be adjusted by goniometers and translation stages. For studies of magnetism, the sample is normally positioned in a cryostat or a cryomagnet - cooling down to temperatures of 0.03 K and appying fields up to 13.2 T.

Analyzer The analyzer is also located in a shielding, but here the reason is to decrease the background in the detector. The crystal holder located again on a goniometer and translation stages allows a horizontal focus of the analyzer, the crystals are mounted to have a fixed vertical focus. The crystals are at the angle Θ_a to the beam, the detector is rotated by $2\Theta_a$.

Detector The neutrons are counted by a beamtube, filled with $^3\mathrm{He}$ under high pressure (ca 10 bar). A neutron can be trapped by a $^3\mathrm{He}$ nucleus and converted to $^4\mathrm{He}$. The emitted γ quant ionizate the gas and is detected like in a Geiger-Müller counter. This allows to count ca. 90% of the incoming neutrons.

Diaphragms, collimators and attenuators In addition to the already described parts several components are needed in the beam path dor beam conditioning. For example variable diaphragms (slits) are installed before and after the sample which are adjusted to the sample size to decrease the background. A secondary shutter is mounted after the monochromator. More diaphragms are with the primary shutter in the reactor wall and between the primary shutter and the monochromator.

Beyond that in every part of the beam path so-called Soller collimators can be applied. It con-

tains of ca. 20 cm long, coated with white GdO_2 foils, which are exactly parallel and therefore limit the divergence of the beam . The value of the divergence is described by the angle α (see fig. 12). Collimators with $\alpha = 15'$ to $\alpha = 60'$ are available. Small divergence corresponds with high resolution but small intensity. The primary collimators are placed in the primary shielding and are changed automatically, the others have to be changed by hand (motorization planned). The beam size is limited only horizontally, i.e. within the scattering plane. For increase of intensity we normally allow a large divergence of the beam in the direction perpendicular to the scattering plane.

Sometimes, e.g. for alignment, the detector is in the straight beam or Bragg reflections have a very large intensity. To avoid a saturation of the detectors, the incoming beam ist attenuated by PE-plates of different thicknesses which can moved into the beam (and combined) automatically.

Monitor To compare or to combine data from different scans or measurements the intensities are normalized to an intensity counted by the monitor in the primary beam. Its signal is proportional to the incoming intensity. This is also important for energy scans, where the incoming intensity changes with $2\Theta_m$ due to the energy-dependent spectrum. Also different reactor power can be corrected in this way (see paragraph 1.9).

Goniometer Monochromator, analyzer and sample are placed on 2-axis goniometers. This allows tilts around two perpendicular to each other which meet in the centre of the beam. So the sample does not move out of the beam centre during the tilt. The available angles are limited ($\pm 15^\circ$), the sample can be adjusted but has to be pre-oriented before measuring on the three-axis instrument. It is also possible to translate the sample a few millimeters horizontally and vertically.

Cover page: Overview over PANDA
From left: Monochromator shielding, sample table with 15T cryomagnet, analyzer box and detector shielding.

Figure 13: *(Following page) Components of PANDA taken in different phases of the construction.*

(a) Side view into the (opened) Monochromator shielding onto the PG-monochromator.

(b) PG-analyzer in the (opened) analyzer box. The horizontal curvature is changed by rotating the individual segments.

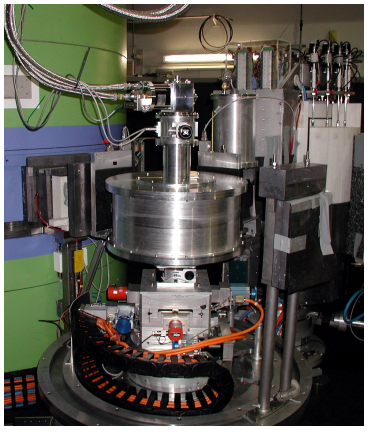

(c) Detailed view onto the sample table with vacuum chamber. From bottom: Rotation table, xy-stage, goniometer, z-stage

(d) Soller collimators in the automatic changer for $\alpha 1$ (in the primary beam.)

(e) Typical sample mounting for use of cryostat.

(f) Detector tubes to be built into the detector shielding

3 Experiment

PANDA is a complex research instrument, where normally measurements on samples at very low temperature, high magnetic fields and / or high pressure are performed. Phonons for example are measured to learn about the interaction potentials in solids. Measurements of spin wave dispersions contribute to determine magnetic interactions.

The goal of this practice is to give inside to the potential of neutron scattering on a three-axis spectrometer. To get results, you have to understand the functionality of the instrument. This can include the alignment of the instrument and the sample. Some data can be taken on a well-known sample, e.g. lead, which can be measured at room temperature (necessary due to the limited time of the practice. A normal experiment needs several days.)

1. Preparation
   - Gather theoretical basics.
   - Generate a strategy for the measurements and a plan of the experiment.
   - Safety instruction at the instrument PANDA.
2. Alignment
   - Proof of the instrument alignment by scans of the monochromator or analyzer axis
   - Determination of the (energy) resolution of the spectrometer for (min.) three different wave vectors by measuring of the incoherent elastic intensity on vanadium. Choose an appropriate configuration for the following measurements.
   - Alignment of the sample, define the scattering plane, optimize background.
   - Perform control scans and learn the use of the user interface on PANDA.
3. Measurements
   - Perform the planned scans to determine the resolution ellipsoid.
   - Measure (min.) one mode of the dispersion relation of lead by different scans.

4 Report

After the experiment you have to report your work. Please explain the experiment and your work in a short way to show how you understand the aim of the different steps. You can prepare this by doing notes during the experiment.

Please analyze the data and interpret it. It is not necessary to repeat the theoretic aspects already discussed in front of the experiment. But your report should be conclusive.

Please:

- Show the measured energy resolution depending on the wave vector. Explain your choice.

- Determine the direction of the resolution ellipsoid, add it to a scheme of the dispersion and show the single scans.
- For the measurements of lead, plot the measured points with the error bars into a dispersion relation(s) and compare to references. Explain how different scan types influence the result.

Finally: please give us a short feedback about the preparation, experiment and support. This can also be done after the experiment. We like to give you an impression about neutron scattering experiments even if practices are complicated. A feedback will help us to improve it for future students.

P.S. Do not forget ruler and calculator.

References

[1] N. W. Ashcroft and N. D. Mermin. *Festkörperpysik*. Oldenbourg, 2001.

[2] B. N. Brockhouse and P. K. Iyengar. Normal modes of germanium by neutron spektrometry. *Phys. Rev.*, 111(3):747, Aug 1958.

[3] W. Demtröder. *Laserspektroskopie*, Kapitel 3 (Linienbreiten und Profile von Spektrallinien). Springer, 4. edition, 2000.

[4] B. Dorner. *Coherent Inelastic Neutron Scattering in Lattice dynamics*. Springer-Verlag, 1982.

[5] K. Dransfeld, P. Kienle, and G. M. Kalvius. *Physik I*, Kapitel 8. Oldenbourg, 8. edition, 1998.

[6] H. Friedrich. *Theoretische Atomphysik*. Springer, 1990.

[7] H. Ibach and H. Lüth. *Festkörperpysik, Einführung in die Grundlagen*. Springer-Verlag, 6. edition, 2002.

[8] J. Kauppinen and J. Partanen. *Fourier Transforms in Spectroscopy*. Wiley-VCH, Berlin, 2001.

[9] C. Kittel. *Einführung in die Festkörperpysik*. Oldenbourg, 10. edition, 1993.

[10] G. Nillson and G. Nellin. Normal vibrations of germanium by neutron spektrometry. *Phys. Rev. B*, 3(2):364, Jan 1971.

[11] G. Shirane, S. m. Shapiro, and J. M. Tranquada. *Neutron scattering with a triple-axis Spektrometer*. Oxford University Press, 2002.

[12] B. T. Willis, editor. *Chemical Applications of Thermal Neutron Scattering*. Oxford University Press, 1973.

[13] R. Zorn. Fourier transforms. In *Neutron Scattering*. T. Brückel, G. Heger, D. Richter and R. Zorn, 2006.

Internet resources

`http://http://www.mlz-garching.de/panda`
: "PANDA" homepage.

`http://www.env-it.de/umweltdaten/`
: Environmental data from the federal Ministry for the Environment, Nature Conservation and Nuclear Safety.

`http://www.umweltdaten.de/utk/kapitel22/E-22-1-2.pdf`
: Estimations of natural and civil exposure in Germany from 1999.

Contact

PANDA

Phone: 089/289-14749
Web: http://www.mlz-garching.de/panda

Astrid Schneidewind

JCNS at Maier-Leibnitz Zentrum Garching, Forschungszentrum Jülich GmbH

Phone: 089/289-14749
e-Mail: Astrid.Schneidewind@frm2.tum.de

Petr Cermak

Phone: 089/289-11773
e-Mail: p.cermak@fz-juelich.de